



OPEN

Optical coherence tomography: A new strategy to image planarian regeneration

SUBJECT AREAS:

ENGINEERING
BIOMEDICAL ENGINEERINGYu-Sheng Lin¹, Chin-Chou Chu¹, Jen-Jen Lin², Chien-Cheng Chang¹, Chun-Chieh Wang^{3,4},
Chiao-Yin Wang^{3,5} & Po-Hsiang Tsui^{3,6}Received
10 March 2014Accepted
11 August 2014Published
10 September 2014Correspondence and
requests for materials
should be addressed to
P.-H.T. (tsuiph@mail.
cgu.edu.tw) or C.-C.C.
(mechang@iam.ntu.
edu.tw)¹Institute of Applied Mechanics, National Taiwan University, Taipei, Taiwan, ²Department of Applied Statistics and Information Science, Ming-Chuan University, Taoyuan, Taiwan, ³Department of Medical Imaging and Radiological Sciences, College of Medicine, Chang Gung University, Taoyuan, Taiwan, ⁴Department of Radiation Oncology, Chang Gung Memorial Hospital, Taoyuan, Taiwan, ⁵Graduate Institute of Clinical Medical Sciences, College of Medicine, Chang Gung University, Taoyuan, Taiwan, ⁶Institute for Radiological Research, Chang Gung University/Chang Gung Memorial Hospital at Linkou, Taoyuan, Taiwan.

The planarian is widely used as a model for studying tissue regeneration. In this study, we used optical coherence tomography (OCT) for the real-time, high-resolution imaging of planarian tissue regeneration. Five planaria were sliced transversely to produce 5 head and 5 tail fragments. During a 2-week regeneration period, OCT images of the planaria were acquired to analyze the signal attenuation rates, intensity ratios, and image texture features (including contrast, correlation, homogeneity, energy, and entropy) to compare the primitive and regenerated tissues. In the head and tail fragments, the signal attenuation rates of the regenerated fragments decreased from -0.2 dB/ μm to -0.05 dB/ μm , between Day 1 and Day 6, and then increased to -0.2 dB/ μm on Day 14. The intensity ratios decreased to approximately 0.8 on Day 6, and increased to between 0.8 and 0.9 on Day 14. The texture parameters of contrast, correlation, and homogeneity exhibited trends similar to the signal attenuation rates and intensity ratios during the planarian regeneration. The proposed OCT parameters might provide biological information regarding cell apoptosis and the formation of a mass of new cells during planarian regeneration. Therefore, OCT imaging is a potentially effective method for planarian studies.

The freshwater planarian *Dugesia japonica* is one of the most common types of planarian and has become a widely used model for investigating regeneration, stem cell biology, and polarity¹⁻⁷. A planarian is able to regenerate completely from tiny tissue fragments of almost any body part, after amputation^{8,9}. If an animal capable of regenerating is sliced laterally, a new head (the anterior region) develops from the anterior-facing wound, and a new tail (the posterior region), develops from the posterior-facing wound¹⁰. The regenerative abilities of a planarian depend on the proliferation and differentiation of pluripotent adult stem cells¹¹ or neoblasts¹²⁻¹⁴. The planarian is useful for studying stem cell biology¹⁵⁻¹⁷, and recent studies have elucidated the molecular mechanisms underlying the maintenance of the planarian adult stem cell population¹⁸, as well as the polarity assignment of new tissue¹⁹, wound-induced injury responses²⁰, stem cell differentiation in regenerating tissues²¹, germ cell biology, and sexual development²²⁻²⁴. Consequently, the use of the planarian as a model in biological research is increasing. In recent years, research groups have used planaria to explore cytoskeletal proteins and phenomena including nervous system regeneration²⁵, and morphogenesis²⁶.

In vivo imaging for real-time monitoring of the morphological and parenchyma changes is highly relevant and has facilitated considerable biological research based on the planarian model. Of the various noninvasive imaging modalities, fluorescence-based techniques are able to image planarians at a cellular resolution. In previous studies, confocal imaging technique have been applied to observe planarians^{21,27}. In addition, the multiphoton microscope is a tool for imaging planarians that has been proposed as the optimal noninvasive means of performing fluorescence microscopy for studying living cells and time-course kinetic applications²⁸. However, planarians display a distinctive light-avoidance behavior known as negative phototaxis²⁹. Therefore, visible light produced during fluorescence imaging may influence their behavior and impede the ability to conduct live imaging of planarian regeneration. Compared with fluorescence techniques and other medical imaging methods (e.g., computed tomography, ultrasound, or magnetic resonance imaging), optical coherence tomography (OCT) is an emerging optical imaging technology for real-time imaging with a spatial resolution of a few micrometers³⁰⁻³². In particular, OCT is based on invisible light. Thus the effects of visible light on the biological behavior of planaria are reduced when employing OCT.



In brief, OCT imaging is based on recording the demodulated pattern generated by interference between the coherent backscattered light derived from a scattering medium, and an optical reference field. Thus, OCT is similar to ultrasound technology, such as that used in B-mode imaging. However, OCT employs low-coherence light instead of sound and produces cross-sectional images by measuring the light backscattered from the tissue. Therefore OCT is potentially suitable for the long-term observation of planarian regeneration without sacrificing the sample. However, the morphological information provided by OCT imaging is insufficient to describe planarian regeneration. Further quantitative information is necessary to supplement OCT imaging regarding tissue parenchyma.

In addition to the signal intensity, an OCT image provides a large amount of information that can be analyzed and used to derive quantitative parameters that provide the means to identify tissue properties. When a light wave propagates in tissue, the absorption and scattering of the light by cells or organs cause the signal attenuation of an OCT image. Previous studies have demonstrated that the attenuation coefficients derived from an OCT image enable the characterizing of scatterers^{33,34}. Texture analysis is also a popular method to extract useful information from images for tissue characterization. Textural analysis has been widely applied in the analysis of OCT images in evaluating the relationship between the image texture and the scatterer properties of biological tissues^{35–37}. In this study, we investigated the feasibility of using the signal attenuation rates, signal intensity ratios, and texture features of OCT images to evaluate planarian regeneration and tissue development.

Results

In Fig. 1, the B-mode OCT images depict the regeneration of a planarian head and tail from Day 1 to Day 14. The OCT image of the planarian is essentially a speckle image, demonstrating that the planarian tissue behaves like a homogeneous medium during OCT imaging. The speckle pattern in the OCT image is caused by the backscattering signals of light, which are dependent on the properties of the scatterers in the planarian tissue. Therefore, to extract the biological information associated with the regeneration of planarian tissue, quantitative analysis of the OCT image is required.

Prior to attenuation analyses, performing tests to clarify the effect of imaging direction on the signal attenuation rate is necessary. Figure 2 shows the signal attenuation rates of the planarian tissue obtained from different imaging directions. The attenuation rates measured using dorsal-to-ventral and ventral-to-dorsal views were -0.25 and -0.22 dB/ μm , respectively. The probability value (p value) obtained from the statistical t test was larger than 0.05, representing that OCT measurement on the planarian is less affected by the imaging direction. Refer to Fig. 1. The planarian under OCT imaging is a homogeneous-like tissue, and thus the imaging direction exerted no significant effect on the OCT measurement of the planaria. In the following experiments, the planaria were imaged from the top (dorsal) to the bottom (ventral) because this entailed a relatively easy measuring process.

Figure 3 shows the changes in the signal attenuation rates measured from the regenerated head and tail fragments. The curve described by the attenuation rate measured from the original tissues enables a comparison with the results of planarian regeneration. The attenuation rate of the regenerated head fragment decreased from approximately -0.2 to -0.05 dB/ μm , from Day 1 to Day 6, and then increased to -0.2 dB/ μm on Day 14. The same trend was observed in the results obtained from the regenerated tails (Fig. 3b). In particular, the p value showed that the signal attenuation rates obtained from the regenerative tissues differed significantly from those of the original tissues ($p < .05$), demonstrating that the signal attenuation rate facilitates effective discrimination between regenerative and original tissues.

Figure 4 depicts the changes in the signal intensity ratios measured from the regenerated head and tail tissues. The signal intensity ratios of the regenerated head and tail tissues decreased from approximately 0.9 to 0.8 on Day 6, and increased to between 0.8 and 0.9 on Day 14. The intensity ratio of the original tissues varied between 0.9 and 1. The characteristics of the signal intensity ratio during planarian regeneration were similar to those of the attenuation rate. The values of the regenerative and original tissues differed significantly ($p < .05$). Moreover, the value of the regenerative fragments gradually approached that of the original tissues.

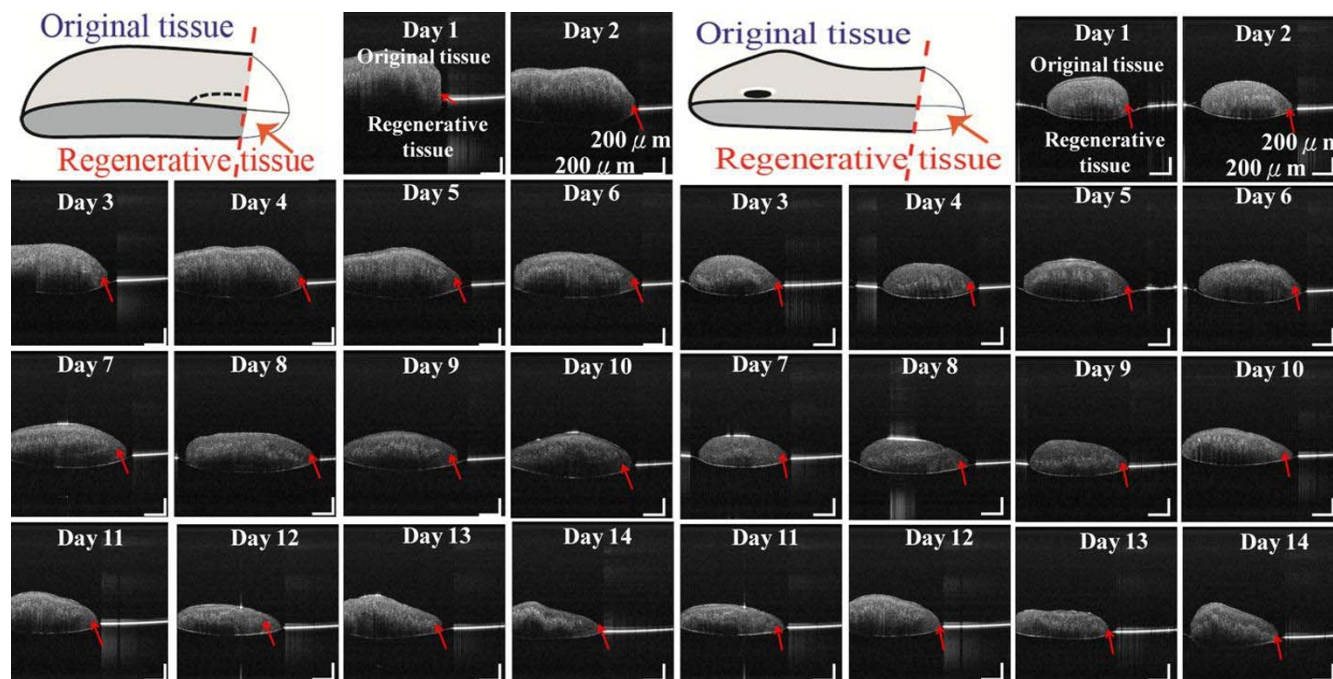


Figure 1 | B-mode images of a planarian, obtained from the axis direction (X-Z plane) during Day 1 to Day 14. (a) Head regeneration and (b) tail regeneration. The portions of the tissue regeneration are indicated by red arrows, and scale bars of 200 μm are included in each figure.

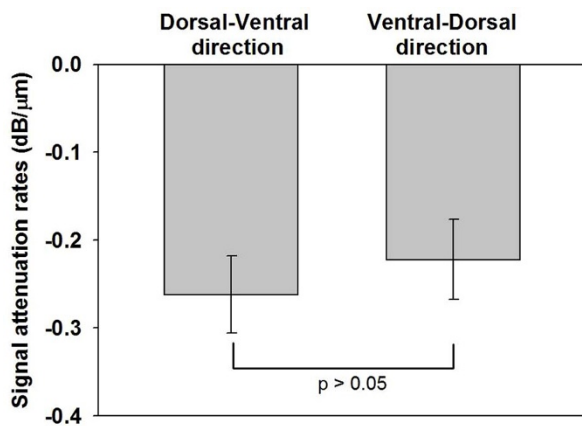


Figure 2 | Signal attenuation rates of the planarian tissue obtained from different imaging directions (imaging from dorsal-to-ventral and ventral-to-dorsal views, respectively).

Using the texture parameters to characterize planarian regeneration is not a satisfactory method, particularly when the performance is compared with that of using the signal attenuation and intensity ratio. Our results demonstrated that the contrast, correlation, and homogeneity exhibited similar trends to those of the attenuation rates and signal intensity ratios (Fig. 5), although the standard deviations of the texture parameters were relatively large ($p < .05$ during regeneration). The energy and entropy were not correlated with the planarian regeneration, as supported by the results shown in Fig. 6 ($p > .05$ during regeneration).

Discussion

The biological mechanism of planaria has been widely explored and is supported by the literature cited in the Introduction section. Few studies have reported the scientific value of imaging planarian regeneration. This study demonstrated that the quantitative analysis of OCT images yields physical and biological results regarding the study of planarian regeneration, providing a solution for studying the dynamics of planarian regeneration in vivo. This paper presents the first successful application of OCT in imaging of planarian regeneration.

The parameters of an OCT image are dependent on the properties of the scatterers in the tissue. In this study, most of the parameters measured using the regenerated tissues differed from those of the original tissues at the early stage of tissue regeneration (between Day

1 and Day 6). The OCT parameters of the regenerated tissues approximated those of the original tissues at subsequent stages of tissue regeneration (between Day 6 and Day 14) indicating that the properties of regenerated planarian tissues might be identical to those of primitive tissues after 2 weeks. According to the morphological observations of the OCT images, planarian tissue regeneration was completed approximately on Day 6 (Fig. 1) when most of the parameter values peaked. Based on the results of the analysis of signal attenuation, intensity ratio, and texture (Figs. 3–6), we suggest that a complete cycle of tissue regeneration in a planarian should not be determined based on morphological information (e.g., size, length, or volume). Considering imaging physics, the measured OCT image parameters are useful indicators of the properties of the regenerated tissues and enable the determination of a complete cycle of planarian tissue regeneration.

When a planarian is injured, a strong muscular contraction occurs immediately to minimize the wound area, which rapidly develops a thin layer of epithelium^{38–40}. Lobo et al. explained that the cycle of planarian tissue regeneration can be divided into 3 stages: (1) closure of the wound within the first 30 to 45 min; (2) formation of a mass of new cells (blasteme) at the injury site, which is visible within 2 to 3 days; and (3) repatterning of the old and new tissues during the subsequent 1 to 2 weeks⁴¹. To explain the biological information obtained using OCT, we discuss how planarian regeneration affects the behavior of light scattering as follows.

The ability to regenerate amputated structures often requires the production of new cells⁴². The new cells can be derived from the amplification and differentiation of resident stem cells, proliferation of differentiated cells, dedifferentiation of cells to a more primitive state, and transdifferentiation of one cell type to another cell type⁴². Cells are the primary scatterers in any light interaction with biological tissue⁴³. However, planaria have apoptosis-related genes and the apoptotic mechanism occurs during tissue regeneration⁴⁴. Thus, the formation of new cells and the occurrence of cell apoptosis can exert an antagonistic effect on the behavior of the scattering of light during regeneration. In the initial regeneration of a planarian, cell apoptosis can be a dominant factor in modulating the behavior of light scattering. Apoptosis is a process of programmed cell death. Once apoptosis is triggered in a cell, shrinkage occurs and the nucleus condensates. The loss of cytoskeleton integrity induces blebbing of the cellular membrane; first, the condensated nucleus fragments and the entire cell disintegrates into apoptotic bodies containing remnants of the nucleus and the other cell components. The nuclear fragmentation can further reduce the scattering cross-sections of the scatterers, decreasing the degree of scattering, enhancing the

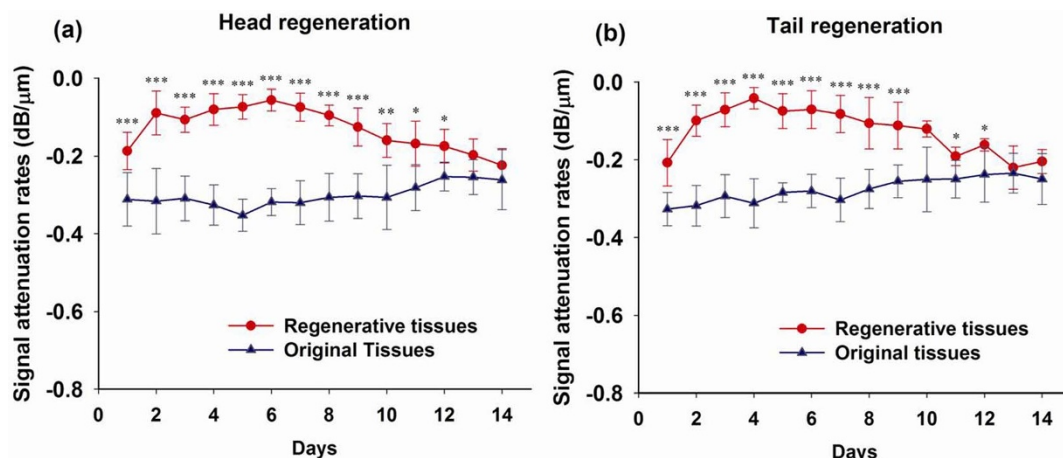


Figure 3 | Signal attenuation rates as a function of planarian regeneration from Day 1 to Day 14. (a) Head regeneration and (b) tail regeneration. Data are expressed as the mean \pm standard deviation. For each day, t tests between the original and regenerative tissues were performed to calculate the p value (* $p < .05$; ** $p < .01$; *** $p < .001$).

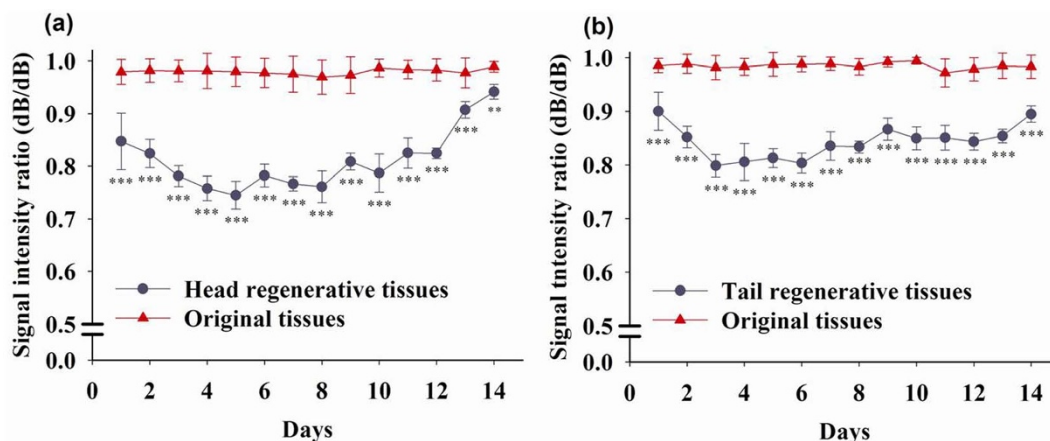


Figure 4 | Signal intensity ratios as a function of planarian regeneration from Day 1 to Day 14. (a) Head regeneration and (b) tail regeneration. Data are expressed as the mean \pm standard deviation. For each day, *t* tests between the original and regenerative tissues were performed to calculate the *p* value (* $p < .05$; ** $p < .01$; *** $p < .001$).

efficiency of light transmission, and decreasing the attenuation of OCT⁴⁵. This might explain why the attenuation rate and the signal intensity of the OCT image decreased from Day 1 to Day 6. The

degree of cell apoptosis gradually decreases after 3 days and then begins to enter the stage of tissue repatterning⁴⁶. The effects of the subsequent biological effects on the OCT imaging are caused by the

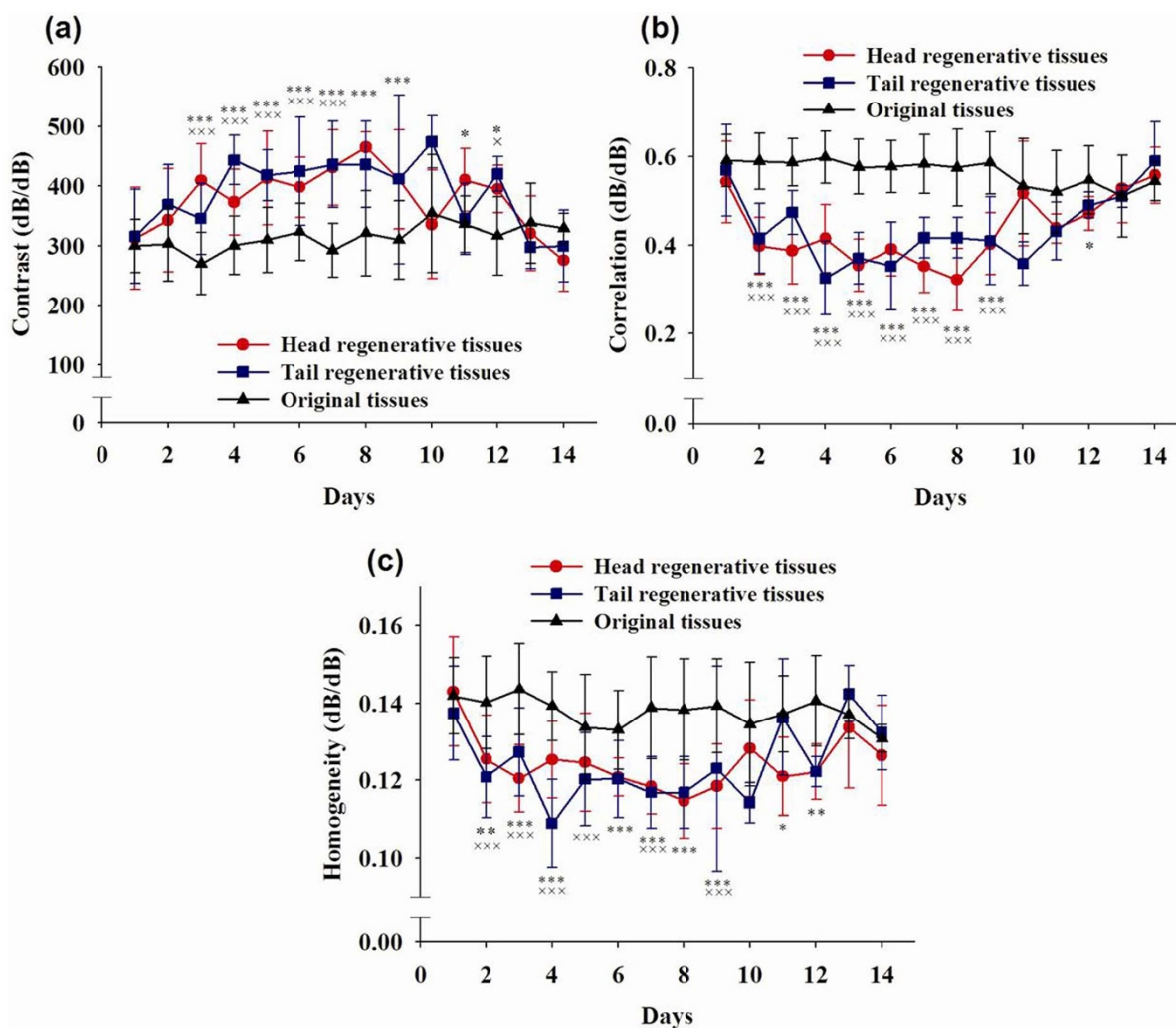


Figure 5 | Textural parameters as a function of planarian regeneration from Day 1 to Day 14. (a) Contrast, (b) correlation, and (c) homogeneity. Data are expressed as the mean \pm standard deviation. Red and blue curves represent the head and tail regenerations, respectively. For each day, *t* tests between the original and regenerative tissues were performed to calculate the *p* value (for head regenerations, * $p < .05$; ** $p < .01$; *** $p < .001$). The symbol *x* represents the statistical analysis for tail regenerations.

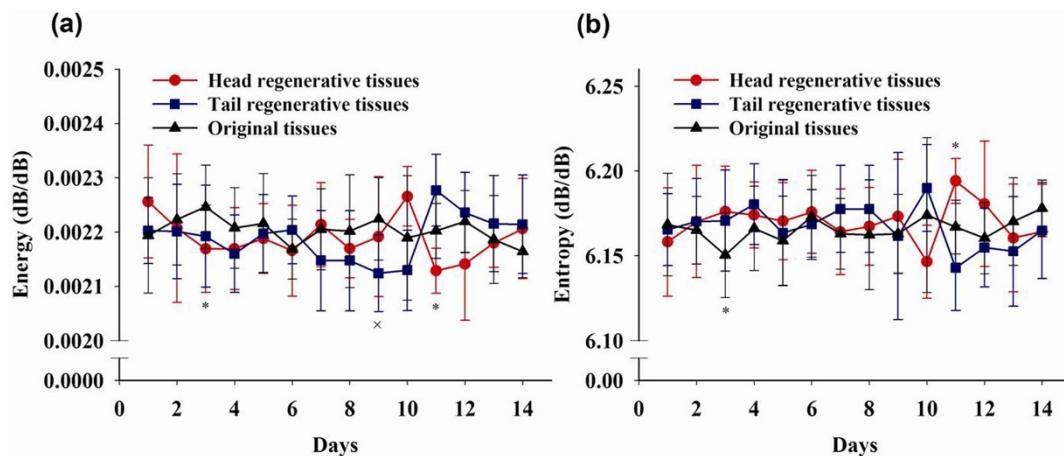


Figure 6 | Textural parameters as a function of planarian regeneration from Day 1 to Day 14. (a) Entropy and (b) energy. Data are expressed as the mean \pm standard deviation. Red and blue curves represent the head and tail regenerations, respectively. For each day, t tests between the original and regenerative tissues were performed to calculate the p value (for head regenerations, * $p < .05$; ** $p < .01$; *** $p < .001$). The symbol x represents the statistical analysis for tail regenerations.

formation of new cells and the finalization of structural developments, increasing both the attenuation rate and the signal intensity.

The results demonstrate that in addition to the signal attenuation rate and intensity ratio, the texture features of contrast, correlation, and homogeneity are useful parameters for evaluating the planarian tissue regeneration (Fig. 5). Contrast is used to describe local variations in the spatial gray-level dependency matrix (SGLDM); correlation describes the probability of the joint occurrence of specified pixel pairs; homogeneity is a measurement of the similarity of the distribution of elements in the SGLDM and the SGLDM diagonal⁴⁷. The contrast typically increased from Day 1 to Day 6, corresponding with an increase in local variations in the image data. The effects of cell apoptosis and the formation of new cells might increase the degree of variation in the scattering cross-sections of the scatterers in the regenerated tissue. A high degree of variation in the scattering cross-sections of the scatterers is expected to reduce the probability of the joint occurrence of the specified pixel pairs and the similarity

in the distribution of elements. Therefore, correlation and homogeneity typically decreased from Day 1 to Day 6. Within the subsequent 1 to 2 weeks of the planarian tissue regeneration, the formation of new cells and the finalization of structural developments increased the scattering wave interference, reducing the contrast and increasing the correlation and homogeneity.

Conclusion

This study investigated planarian regeneration using OCT imaging in real time. The results demonstrate that OCT imaging enables the in vivo observation of planarian regeneration at a high spatial resolution. The OCT image-based quantitative parameters, including signal attenuation rate, intensity ratio, and texture feature parameters, provide information on cell apoptosis and the formation of new cells during the process of tissue regeneration. Regarding future planarian studies, OCT imaging has the potential to be applied in the investigation of tissue regeneration.

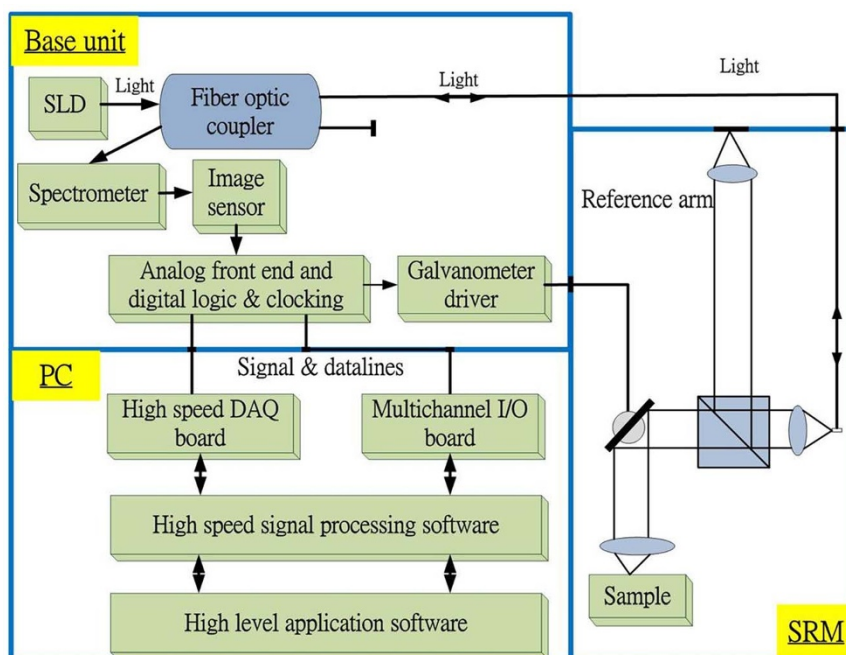


Figure 7 | Diagrammatic representation of the real-time OCT imaging system used for evaluating planarian regeneration.

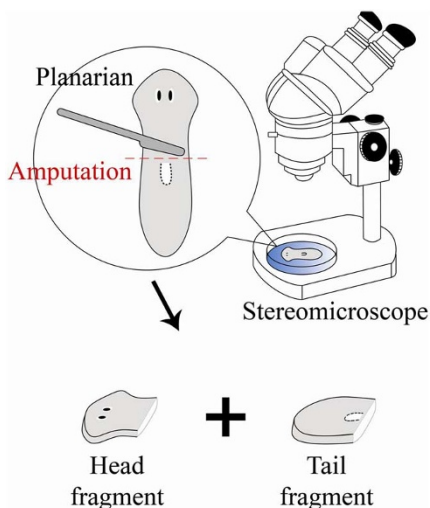


Figure 8 | Illustration of planarian slicing performed under a stereomicroscope (this figure was created by YSL, using the Illustrator software).

Methods

OCT system. Figure 7 depicts a schema of the standard Spectral Radar-OCT (SR-OCT) system (Model OCP930SR, Thorlabs Inc., Newton, NJ, USA) used in this study, including a base unit, a PC, and a spectral radar microscope (SRM). The base unit contains a broadband super luminescent diode, which is located inside the SRM and guides the light into a Michelson interferometer where it is split along 2 separate optical paths. The 2 optical paths, microscope light and reference light, travel through the same fiber to the spectrometer and imaging sensor inside the base unit. Data acquisition and processing are performed by the SR-OCT software package, and the resulting images are displayed on the PC at up to 8 frames per second. The wavelength of the light source is approximately 930 nm, and the peak power output is 2 mW. The axial and lateral resolutions of the system are 3.1 and 4 μm , respectively. The estimated refractive index for soft tissue is 1.4⁴⁸.

Planarian regeneration measurements using optical coherence tomography

imaging. The planaria were collected in the Wufongchi Scenic Area in Taiwan (GPS coordinates: 24.832796, 121.746368) and no specific permissions were required, because the field studies did not involve endangered or protected species. The planaria were between 3 mm and 7 mm in length, and were starved for 1 week in the laboratory. Prior to the experiments, the planaria were placed in a chlorotone solution (with a concentration of 0.1%–0.2%) at a temperature of approximately 4°C for 10-min to anesthetize them⁴⁹. The planaria were sliced laterally using a scalpel and a stereo microscope (Model S8 APO, Leica Microsystems, Wetzlar, Germany) to obtain head and tail (including the pharynx) fragments, as shown in Fig. 8. To enable tissue regeneration, the fragments were then bred in a tissue-culture plate filled with fresh media (aerated water) in the dark, at 19°C, for a period of 2 weeks.

In this study, 10 planaria fragments were evaluated, comprising 5 head and 5 tail fragments. For measurements, each fragment was removed from the tissue-culture plate and placed on a moist filter paper to prevent it from drying out. The OCT system

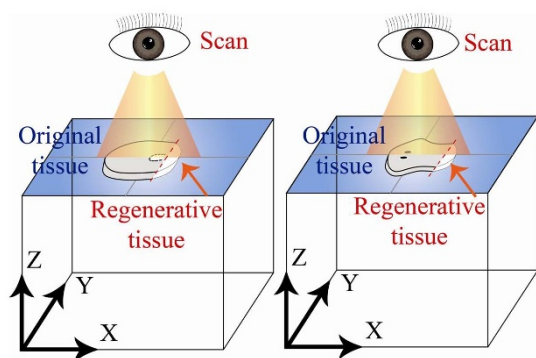


Figure 9 | Diagrammatic representation of a planarian undergoing OCT scanning and imaging. (a) The tail fragment was scanned in the axis direction (X-Z plane) after transverse amputation; (b) The head fragment was scanned in the axis direction (X-Z plane) after transverse slicing (this figure was created by YSL using the Illustrator software).

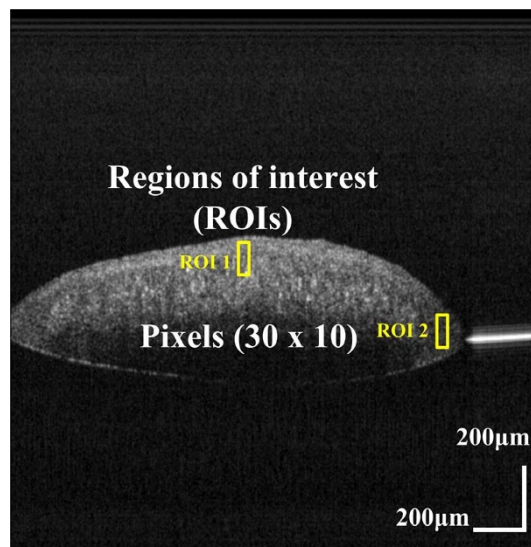


Figure 10 | A typical B-mode OCT image of a planarian scanned in the axis direction. The pixel data in ROIs 1 and 2 (with a size of 30 \times 10 pixels) corresponding to the original and regenerative tissues, respectively, were used for the quantitative analysis of the OCT images.

was used to acquire cross-sectional images in the axis direction (X-Z plane) of the planarian regeneration fragment, as illustrated in Fig. 9. The size of the acquired OCT image was 512 \times 500 pixels, corresponding to a depth and width of 1.59 mm and 2 mm, respectively. For each fragment, the OCT image was recorded every 2 days to observe the tissue regeneration.

A typical B-mode image of a planarian obtained using OCT is shown in Fig. 10. According to manufacturer specifications of the OCT system, the signal-to-noise ratio (SNR) of an image can reach 20 dB or higher. This means that the amplitude of the OCT signal is at least 100 times that of the noise signal, resulting in a sufficient image quality. In a high-SNR environment, the signals are not easily affected by noise and multiple scattering, making estimations of quantitative parameters reliable.

Data analysis. The OCT images were used to estimate the attenuation rate, signal intensity ratio, and texture parameters. Two regions of interests (ROIs) with a size of 30 \times 10 pixels (Fig. 10) were used to collect pixel data from the original (ROI 1) and regenerative tissues (ROI 2). The signal attenuation rates of the original and regenerative tissues were calculated by determining the slopes of the line of best fit derived from the scan lines in ROIs 1 and 2, respectively. Line fitting based on the least squares method was implemented using the SigmaPlot program (Version 9, Systat Software, Inc., San Jose, CA, USA). The signal intensity ratio for the regenerative tissues was calculated using the average pixel value of the regenerative tissue (ROI 2) divided by that of the original tissue (ROI 1). The ROI 1 was divided into two sub-ROIs to calculate the signal intensity ratio of the original tissues. Meanwhile, the pixel data in the ROIs 1 and 2 were used to calculate five texture parameters, including contrast, correlation, homogeneity, energy, and entropy. The texture analysis of the OCT image was performed using the built-in functions of Matlab software (Version 7.0.1, The MathWorks, Inc., Natick, MA, USA).

- Oviedo, N. J. *et al.* Long-range neural and gap junction protein-mediated cues control polarity during planarian regeneration. *Dev. Biol.* **339**, 188–199 (2010).
- Evans, D. J., Owlarn, S., Tejada Romero, B., Chen, C. & Aboobaker, A. A. Combining classical and molecular approaches elaborates on the complexity of mechanisms underpinning anterior regeneration. *PLoS One* **6**, e27927; DOI: 10.1371/journal.pone.0027927 (2011).
- Umesono, Y., Tasaki, J., Nishimura, K., Inoue, T. & Agata, K. Regeneration in an evolutionarily primitive brain - the planarian *Dugesia japonica* model. *Eur. J. Neurosci.* **34**, 863–869 (2011).
- Sánchez Alvarado, A. Regeneration and the need for simpler model organisms. *Philos. Trans. R. Soc. Lond. B Biol. Sci.* **359**, 759–763 (2004).
- Agata, K. *et al.* Structure of the planarian central nervous system (CNS) revealed by neuronal cell markers. *Zoolog. Sci.* **15**, 433–440 (1998).
- Beane, W. S., Morokuma, J., Lemire, J. M. & Levin, M. Bioelectric signaling regulates head and organ size during planarian regeneration. *Development* **140**, 313–322 (2013).
- Saló, E. & Bagañá, J. Regeneration and pattern formation in planarians. I. The pattern of mitosis in anterior and posterior regeneration in *Dugesia (G) tigrina*, and a new proposal for blastema formation. *J. Embryol. Exp. Morphol.* **83**, 63–80 (1984).
- Agata, K. Regeneration and gene regulation in planarians. *Curr. Opin. Genet. Dev.* **13**, 492–496 (2003).



9. Agata, K., Tanaka, T., Kobayashi, C., Kato, K. & Saitoh, Y. Intercalary regeneration in planarians. *Dev. Dyn.* **226**, 308–316 (2003).
10. Morgan, T. H. Experimental studies of the regeneration of planaria maculate. *Arch. Entw. Mech. Org.* **7**, 364–397 (1898).
11. Agata, K. & Umeson, Y. Brain regeneration from pluripotent stem cells in planarians. *Philos. Trans. R. Soc. B Biol. Sci.* **363**, 2071–2078 (2008).
12. Bagaña, J. Planarian neoblasts. *Nature* **290**, 14–15 (1981).
13. Bagaña, J., Salo, E. & Auladell, C. Regeneration and pattern formation in planarians III. Evidence that neoblasts are totipotent stem cells and the source of blastema cells. *Development* **107**, 77–86 (1989).
14. Shibata, N., Rouhana, L. & Agata, K. Cellular and molecular dissection of pluripotent adult somatic stem cells in planarians. *Dev. Growth Differ.* **52**, 27–41 (2010).
15. Newmark, P. A. & Sánchez Alvarado, A. Not your father's planarian: a classic model enters the era of functional genomics. *Nat. Rev. Genet.* **3**, 210–219 (2002).
16. Sánchez Alvarado, A., Newmark, P. A., Robb, S. M. & Juste, R. The *Schmidtea mediterranea* database as a molecular resource for studying platyhelminthes, stem cells and regeneration. *Development* **129**, 5659–5665 (2002).
17. Wagner, D. E., Wang, I. E. & Reddien, P. W. Clonogenic neoblasts are pluripotent adult stem cells that underlie planarian regeneration. *Science* **332**, 811–816 (2011).
18. Wagner, D. E., Ho, J. J. & Reddien, P. W. Genetic regulators of a pluripotent adult stem cell system in planarians identified by RNAi and clonal analysis. *Cell Stem Cell* **10**, 299–311 (2012).
19. Petersen, C. P. & Reddien, P. W. A wound-induced Wnt expression program controls planarian regeneration polarity. *Proc. Natl. Acad. Sci. USA* **106**, 17061–17066 (2009).
20. Wenemoser, D., Lapan, S. W., Wilkinson, A. W., Bell, G. W. & Reddien, P. W. A molecular wound response program associated with regeneration initiation in planarians. *Genes Dev.* **26**, 988–1002 (2012).
21. Eisenhoffer, G. T., Kang, H. & Sánchez Alvarado, A. Molecular analysis of stem cells and their descendants during cell turnover and regeneration in the planarian *Schmidtea mediterranea*. *Cell Stem Cell* **3**, 327–339 (2008).
22. Newmark, P. A., Wang, Y. & Chong, T. Germ cell specification and regeneration in planarians. *Cold Spring Harb. Symp. Quant. Biol.* **73**, 573–581; DOI: 10.1101/sqb.2008.73.022 (2008).
23. Wang, Y., Stary, J. M., Wilhelm, J. E. & Newmark, P. A. A functional genomic screen in planarians identifies novel regulators of germ cell development. *Genes Dev.* **24**, 2081–2092 (2010).
24. Wang, Y., Zayas, R. M., Guo, T. & Newmark, P. A. Nanos function is essential for development and regeneration of planarian germ cells. *Proc. Natl. Acad. Sci. USA* **104**, 5901–5906 (2007).
25. Gentile, L., Cebrià, F. & Bartscherer, K. The planarian flatworm: an in vivo model for stem cell biology and nervous system regeneration. *Dis. Model Mech.* **4**, 12–19 (2011).
26. Fagotti, A., Simoncelli, F., Rosa, I. D. & Pascolini, R. Cytoskeletal proteins and morphogenesis in planarians. *ISJ* **3**, 118–124 (2006).
27. Zhu, S. J. & Pearson, B. J. The retinoblastoma pathway regulates stem cell proliferation in freshwater planarians. *Dev. Biol.* **373**, 442–452 (2013).
28. Zipfel, W. R., Williams, R. M. & Webb, W. W. Nonlinear magic: multiphoton microscopy in the biosciences. *Nat. Biotechnol.* **21**, 1369–1377 (2003).
29. Inoue, T. *et al.* Morphological and functional recovery of the planarian photosensing system during head regeneration. *Zool. Sci.* **21**, 275–283 (2004).
30. Fischer, M. D. *et al.* Noninvasive, in vivo assessment of mouse retinal structure using optical coherence tomography. *PLoS One* **4**, e7507; DOI: 10.1371/journal.pone.0007507 (2009).
31. Serbecic, N. *et al.* High resolution spectral domain optical coherence tomography (SD-OCT) in multiple sclerosis: the first follow up study over two years. *PLoS One* **6**, e19843; DOI: 10.1371/journal.pone.0019843 (2011).
32. Lin, Y. S., Chu, C. C., Tsui, P. H. & Chang, C. C. Evaluation of zebrafish brain development using optical coherence tomography. *J. Biophotonics* **6**, 668–678 (2013).
33. Popescu, D. P., Flueraru, C., Mao, Y., Chang, S. & Sowa, M. G. Signal attenuation and box-counting fractal analysis of optical coherence tomography images of arterial tissue. *Biomed. Opt. Express* **1**, 268–277 (2010).
34. Smithies, D. J., Lindmo, T., Chen, Z., Nelson, J. S. & Milner, T. E. Signal attenuation and localization in optical coherence tomography studied by Monte Carlo simulation. *Phys. Med. Biol.* **43**, 3025–3044 (1998).
35. Baroni, M., Diciotti, S., Evangelisti, A., Fortunato, P. & Torre, A. L. Texture classification of retinal layers in optical coherence tomography. *IFMBE Proceedings* **16**, 847–850 (2007).
36. Chen, Y. *et al.* Effects of axial resolution improvement on optical coherence tomography (OCT) imaging of gastrointestinal tissues. *Opt. Express* **16**, 2469–2485 (2008).
37. Garcia-Allende, P. B. *et al.* Morphological analysis of optical coherence tomography images for automated classification of gastrointestinal tissues. *Biomed. Opt. Express* **2**, 2821–2836 (2011).
38. Bagaña, J. *et al.* Regeneration and pattern formation in planarians: cells, molecules and genes. *Zool. Sci.* **11**, 781–795 (1994).
39. Pascolini, R., Tei, S., Vagnetti, D. & Bondi, C. Epidermal cell migration during wound healing in *Dugesia lugubris*. Observations based on scanning electron microscopy and treatment with cytochalasin. *Cell Tissue Res.* **236**, 345–349 (1984).
40. Sánchez Alvarado, A. & Newmark, P. A. The use of planarians to dissect the molecular basis of metazoan regeneration. *Wound Repair Regen.* **6**, 413–420 (1998).
41. Lobo, D., Beane, W. S. & Levin, M. Modeling Planarian Regeneration: A primer for reverse-engineering the worm. *PLoS Comput. Biol.* **8**, e1002481; DOI: 10.1371/journal.pcbi.1002481 (2012).
42. King, R. S. & Newmark, P. A. The cell biology of regeneration. *J. Cell Biol.* **196**, 553–562 (2012).
43. Wang, L. V. & Wu, H. I. *Biomedical optics: principles and imaging* (John Wiley & Sons, Hoboken, New Jersey, 2007).
44. Hwang, J. S., Kobayashi, C., Agata, K., Ikeo, K. & Gojobori, T. Detection of apoptosis during planarian regeneration by the expression of apoptosis-related genes and TUNEL assay. *Gene* **333**, 15–25 (2004).
45. van der Meer, F. J. *et al.* Apoptosis- and necrosis-induced changes in light attenuation measured by optical coherence tomography. *Lasers Med. Sci.* **25**, 259–267; DOI: 10.1007/s10103-009-0723-y (2010).
46. Pelletier, J. *et al.* Cell death and tissue remodeling in planarian regeneration. *Dev. Biol.* **338**, 76–85 (2010).
47. Gossage, K. W., Tkaczyk, T. S., Rodriguez, J. J. & Barton, J. K. Texture analysis of optical coherence tomography images: feasibility for tissue classification. *J. Biomed. Opt.* **8**, 570–575 (2003).
48. Tearney, G. J. *et al.* Determination of the refractive index of highly scattering human tissue by optical coherence tomography. *Opt. Lett.* **20**, 2258–2260 (1995).
49. Guedelhofer IV, O. C. & Sánchez Alvarado, A. Planarian immobilization, partial irradiation, and tissue transplantation. *J. Vis. Exp.* **66**, e4015; DOI: 10.3791/4015 (2012).

Acknowledgments

This work was supported by the Ministry of Science and Technology (Taiwan) under Grant No. MOST 103-2221-E-182-001-MY3 and the Chang Gung Memorial Hospital (Linkou, Taiwan) under Grant No. CMRPD1C0711. This work was also supported by the Chang Gung Medical Research Program (CMRP) for Proton Therapy Basic Research (Grant Nos. CMRPD1C0661 and CMRPD1C0641). The funders had no role in study design, data collection and analysis, decision to publish, or preparation of the manuscript.

Author contributions

Y.S.L., J.J.L. and P.H.T. wrote the manuscript text and performed data analysis. C.C.C. and C.C.C. provided experimental materials and facilities. C.C.W. and C.Y.W. performed experiments and prepared figures. All authors reviewed the manuscript.

Additional information

Competing financial interests: The authors declare no competing financial interests.

How to cite this article: Lin, Y.-S. *et al.* Optical coherence tomography: A new strategy to image planarian regeneration. *Sci. Rep.* **4**, 6316; DOI:10.1038/srep06316 (2014).



This work is licensed under a Creative Commons Attribution-NonCommercial-NoDerivs 4.0 International License. The images or other third party material in this article are included in the article's Creative Commons license, unless indicated otherwise in the credit line; if the material is not included under the Creative Commons license, users will need to obtain permission from the license holder in order to reproduce the material. To view a copy of this license, visit <http://creativecommons.org/licenses/by-nc-nd/4.0/>